NANO LETTERS

Letter

pubs.acs.org/NanoLett

Photoelectron Spectroscopy of CdSe Nanocrystals in the Gas Phase: A Direct Measure of the Evanescent Electron Wave Function of Quantum Dots

Wei Xiong,*[,†] Daniel D. Hickstein,[†] Kyle J. Schnitzenbaumer,[‡] Jennifer L. Ellis,[†] Brett B. Palm,[§] K. Ellen Keister,[†] Chengyuan Ding,[†] Luis Miaja-Avila,[∥] Gordana Dukovic,[‡] Jose L. Jimenez,[§] Margaret M. Murnane,[†] and Henry C. Kapteyn[†]

[†]Department of Physics and JILA, University of Colorado and NIST, Boulder, Colorado 80309, United States

[‡]Department of Chemistry and Biochemistry, University of Colorado, Boulder, Colorado 80309, United States

[§]Department of Chemistry and Biochemistry and CIRES, University of Colorado, Boulder, Colorado 80309, United States

[∥]Quantum Electronics and Photonics Division, NIST, Boulder, Colorado 80305, United States

S *Supporting Information*

ABSTRACT: We present the first photoelectron spectroscopy measurements of quantum dots (semiconductor nanocrystals) in the gas phase. By coupling a nanoparticle aerosol source to a femtosecond velocity map imaging photoelectron spectrometer, we apply robust gas-phase photoelectron spectroscopy techniques to colloidal quantum dots, which typically must be studied in a liquid solvent or while bound to a surface. Working with a flowing aerosol of quantum dots offers the additional advantages of providing fresh nanoparticles for each laser shot and removing perturbations from bonding with a surface or interactions with the solvent. In this work, we perform a two-photon photoionization experiment to show that the photoelectron yield per exciton depends on the physical size of the quantum dot, increasing for smaller dots. Next, using effective mass modeling we show that the extent to which the electron wave function of the exciton extends from the quantum dot, the so-called "evanescent electron wavefunction", increases as the size of the quantum dot decreases. We show that the photoelectron yield is dominated by the evanescent electron density due to quantum confinement effects, the difference in the density of states inside and outside of the quantum dots, and the angle-dependent transmission probability of electrons through the surface of the quantum dot. Therefore, the photoelectron yield directly reflects the fraction of evanescent electron wave function that extends outside of the quantum dot. This work shows that gas-phase photoelectron spectroscopy is a robust and general probe of the electronic structure of quantum dots, enabling the first direct measurements of the evanescent exciton wave function.

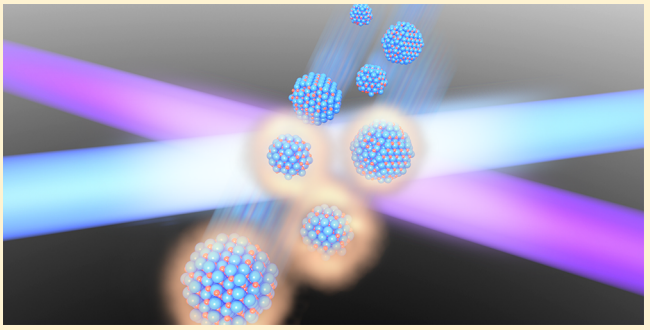

KEYWORDS: *Quantum dots, ultrafast, electronic structure, aerodynamic lens, gas phase photoelectron spectroscopy, velocity map imaging*

Quantum dots (QDs) are one of the fundamental building blocks of complex nanoscale devices, including next-generation solar energy harvesters,[1−6] quantum computers,[7] and nanoelectromechanical systems.[8] To effectively design nanosystems, a thorough understanding of the electronic coupling between QDs and the substrate material is needed. Electronic coupling between QDs is highly dependent on the overlap between exciton wave functions. The extent of this overlap is dictated by the portion of the exciton wave function that extends outside the physical boundary of QDs,[1,9−12] which we refer to as the "evanescent electron wavefunction".

To date, the delocalization of the nanocrystal excited-state electron wave function has been measured by indirect experimental methods. One method to quantify the exciton delocalization is to measure the shifts of absorption peaks, which provide information about electronic coupling between adjacent QDs,[13,14] allowing the extent of exciton orbital overlap to be inferred in an indirect manner. In other studies, researchers have used ultrafast transient absorption spectroscopy to show that the charge separation rate of Type II core−shell QDs depends on the extent of the evanescent exciton wave functions in the shell portion of the core−shell QDs.[10,11,15,16] However, none of these studies provides a direct probe of the evanescent electron wave function.

Received: April 12, 2013
Revised: May 16, 2013
Published: May 20, 2013

   dx.doi.org/10.1021/nl401309z | *Nano Lett.* 2013, 13, 2924−2930

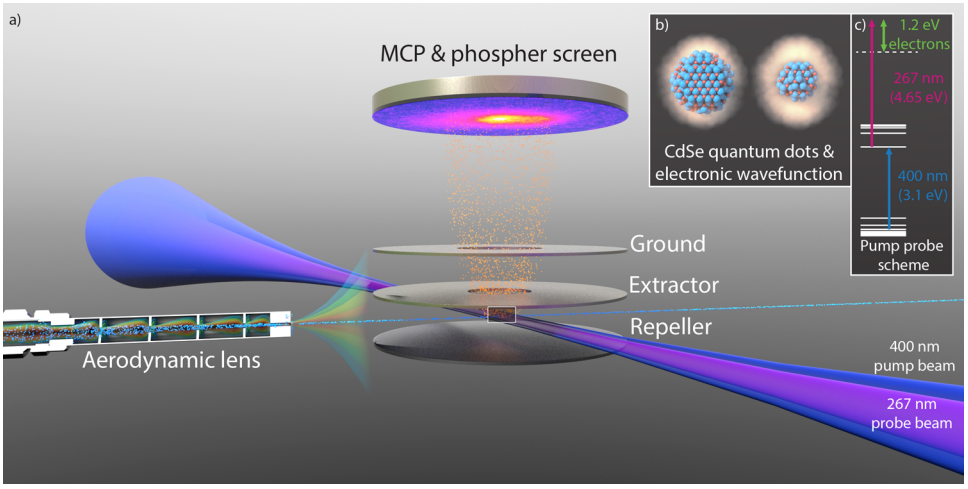

Figure 1. (a) The experimental apparatus consists of a velocity map imaging photoelectron spectrometer coupled to a nanoparticle aerosol source. Clusters of quantum dots (QDs) are focused into the interaction region by an aerodynamic lens, where they are excited and ionized by two time-delayed 40 fs laser pulses. (b) Smaller quantum dots that have been excited to an exciton state have an electronic wave function that extends further outside of the QD and are therefore easier to ionize. (c) In the two-photon photoelectron spectroscopy (2PPE) experiment, the 400 nm pump pulse excites an electron from the valence band to the conduction band. After a time delay, the 267 nm probe pulse brings the electron into the continuum with ~1.2 eV of kinetic energy.

Photoelectron spectroscopy provides electronic structure information that is complementary to that obtained from transient absorption spectroscopy.[10,17−24] While a transient absorption experiment probes both the initial state and the final state simultaneously, photoelectron spectroscopy liberates an electron into a plane-wave state, thereby making a direct measurement of only the initial state. Additionally, photoelectron spectroscopy can access states that are dark (forbidden) in optical spectroscopy.[25−30] Surface photoelectron spectroscopy has been used to infer the delocalization of exciton wave functions indirectly by comparing the photoelectron yield of both core-only CdSe and core−shell CdSe/ZnS QDs on a gold surface.[31] In that work, Naaman and coworkers found that a ZnS shell can effectively screen the interaction between the exciton states and the surface states only for QDs with large diameters. This behavior was attributed to the fact that the electron wave functions for the smaller dots extend further from the core and are able to penetrate the shell material. Other recent work has shown that photoelectron spectroscopy can be used to detect both hot exciton decay and multiexciton generation in PbS quantum dots prepared on a gold surface,[25] demonstrating the ability of time-resolved photoelectron spectroscopy to study exciton dynamics in nanoscale systems.

In this Letter, we present the first study of QDs in the gas phase, which isolates the QDs from substrates and solvents and thereby eliminates the effects of external interactions and bonding. We use an aerosol sample of CdSe QDs that is constantly refreshed in the interaction region, so that new QDs are used for each laser shot, which avoids problems associated with charging, photo-oxidation and other sample degradations.[32−35] This new experimental capability allows us to show that the total photoelectron yield from the QDs is proportional to the fraction of the photoexcited electron wave function that extends outside the QD, thereby making the first direct measurement of the evanescent electron density of the QD exciton. We use ultrafast two-photon photoelectron spectroscopy (2PPE) to first create an exciton in a QD and then subsequently liberate an electron using a second photon. By using a photoelectron spectrometer and adjusting the time-delay between the two pulses, we can collect angle, energy, and time-resolved photoelectron spectra of the QD excitons. We observe that the total photoelectron yield per exciton is inversely proportional to the size of the QDs. Using effective mass modeling[9,11,12] and the three-step model of photoemission from bulk material,[26,27,36] we demonstrate that the size dependence of the photoelectron yield can be explained by the extent to which the exciton wave function extends outside the QD (Figure 1b). In this regard, photoemission from QDs is more similar to photoemission from molecules rather than bulk materials. In the future, by using this general approach to better understand the various factors influencing exciton delocalization and coupling, complex nanostructures can be designed for better charge transfer efficiency.

Methods. In order to reach sufficient aerosol concentrations in the high-vacuum chamber, we utilize an aerodynamic lens. Since its invention in 1995,[37] the aerodynamic lens has transformed the field of aerosol and atmospheric sciences by enabling the development of aerosol mass spectrometers,[38,39] which can measure the chemical composition of size-selected particles in the atmosphere. While several previous studies have coupled an aerodynamic lens with a photoelectron spectrometer to study nanoparticles made from dielectric materials such as NaCl[40] and SiO_2,[41] this work represents the first time that an aerodynamic-lens equipped photoelectron spectrometer has been used to study semiconductor nanomaterials and also presents the first time-resolved photoelectron spectroscopy of nanoparticles in the gas phase.

The experimental apparatus consists of a velocity map imaging (VMI) photoelectron spectrometer[42,43] coupled to a nanoparticle generator and an aerodynamic lens (Aerodyne),[44] which introduce particles into the interaction region[40,41] (Figure 1a). The octadecylamine capped CdSe QDs (NN-Labs) are diluted to 0.01 mg/mL under argon using hexane as a solvent but otherwise used as received. The sizes of the quantum dots (2.3, 2.5, and 2.8 nm) were determined from the band-edge absorption using the tuning curve provided by the

dx.doi.org/10.1021/nl401309z | Nano Lett. 2013, 13, 2924−2930

manufacturer, in good agreement with previously published relationships.[45]

The hexane solution containing the QDs is aerosolized by a compressed-gas atomizer (TSI inc.) with helium gas to form droplets of ~1 μm diameter. The droplets are allowed to dry before entering the aerodynamic lens, leaving behind clusters of quantum dots with an average diameter of 50 nm. The quantum confined properties of the QD clusters are well preserved after the aerosol system, as observed using UV–visible spectroscopy (Supporting Information Figure S1). The isolation of the individual QDs within the larger clusters indicates that the ligands remain attached to the QDs during the atomization process and subsequent expansion into the vacuum. For dynamic measurements such as optical transient absorption or surface two-photon photoemission spectroscopies (which of necessity probe the interaction region with many laser shots), the sample must be continuously refreshed using flowing or rotating sample cells[18] in order to avoid effects such as long-lived trap states and optical blinking in the quantum dots.[46,47] Sample degradation is not a problem in this gas-phase experiment, because the particles are flowing through the system and new QDs are used for every measurement. The QD aerosol is collimated to a width of approximately 500 μm by an aerodynamic lens, which creates a nanoparticle beam by passing the QD–helium aerosol through a series of six orifices with decreasing diameters from 5 to 3 mm. The collimated cluster beam is introduced into the first vacuum chamber and then passes through a 1.5 mm skimmer into a separate, differentially pumped, VMI vacuum chamber.[43]

In the 2PPE experiment (Figure 1c), the QDs are first excited by a 400 nm pump pulse (40 fs) and the resulting dynamics are then probed using a 267 nm pulse (40 fs). Both beams are derived from a 1 kHz Ti:sapphire 800 nm laser (KMLabs) using BBO crystals, and the time delay between them is controlled using a Mach–Zehnder interferometer. The power and polarization of each beam is controlled by a half-wave plate and a polarizer. The photon flux of the 400 nm beam is set to approximately 0.05 mJ/cm^2, which is well below the single exciton limit for all the quantum dots in this study[17,48] (Supporting Information Section 3). The polarization for both beams is set parallel to the plane of the detector. The photoelectrons are focused onto an MCP/phosphor detector by three electrodes in the standard Eppink–Parker geometry.[42] A CCD camera captures the photoelecton images (Supporting Information Figure S2), which are then reconstructed using the BASEX algorithm of Dribinski and co-workers.[49] For each time-resolved experiment shown in this paper, the data acquisition time is about 30 min. We estimate that there are 10^7 particles in our interaction volume (Supporting Information Section 3), which is a much lower number of particles than that used for other measurements. For instance, transient absorption spectroscopy typically requires 10^{10} particles in the interaction region.[50] This comparison shows that photoelectron spectrosopy can provide better sensitivity, which allows for the study of lower concentration samples.

Single band effective mass model calculations[9,11,12] were carried out to understand the evanenscent wave functions of electrons and holes in QDs with different diameters. In these calculations, photoexcitation of the CdSe QDs is modeled as an electron (hole) in a spherically symmetric finite potential defined by the conduction (valence) band potential of bulk CdSe. After solving for the carrier confinement energies, the calculated radial carrier densities are normalized such that the sum of the spherically integrated carrier density is equal to one. A detailed description of these calculations is found in the Supporting Information (Section 4).

Results: Inverse Scaling of the Photoelectron Yield with QD Size. The time-resolved 2PPE spectrum from the 2.3 nm CdSe QDs (Figure 2a) shows a broad peak near 1.2 eV that

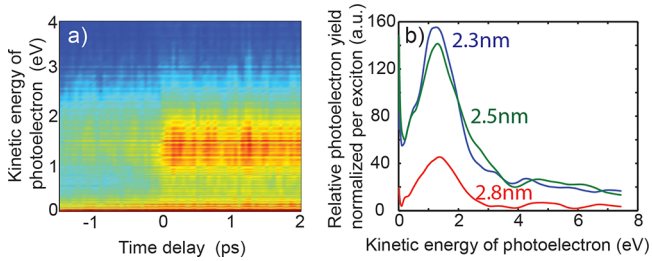

Figure 2. Two-photon photoelectron spectroscopy (2PPE) from exciton states of CdSe QDs. (a) The temporal evolution of the 2PPE spectra from 2.3 nm diameter CdSe QDs shows a broad peak corresponding to the 1S electron state. (b) Relative photoelectron yield per exciton for different diameter CdSe QDs, observed with a pump–probe time delay of 50 fs. The time independent signal has been subtracted, as detailed in Supporting Information Section 2. The total photoelectron yield per exciton decreases as the QD diameter increases from 2.3 to 2.8 nm.

exists for positive time delays, that is, when the 400 nm pump pulse precedes the 267 nm probe pulse. This peak does not decay appreciably on the ~100 ps time scale explored in this study. The less intense features at negative time delays, when the probe pulse precedes the pump pulse, are time independent and result from ionization from either the 267 or 400 nm beams acting alone. The 2PPE spectra of 2.5 and 2.8 nm QDs show a very similar behavior (Supporting Information Figures S4b, S4c). A control experiment using only octadycelamine ligands dissolved in hexane demonstrates that the signal from both ligands and solvent is negligible (Supporting Information Figure S5). The sharp peak at zero kinetic energy results from electrons that are first excited to loosely bound states near the continuum by the probe pulse and then ionized by the DC field of the spectrometer,[51] similar to a zero kinetic energy (ZEKE) experiment.

For each size QDs, the 2PPE spectrum at positive time delays (Figure 2b) shows a peak centered at 1.2 ± 0.1 eV, which, given our probe photon energy of 4.65 eV, corresponds to an exciton state where the electron lies at −3.45 eV with respect to vacuum (Figure 1c). Effective mass calculations show that the 1S electron should be bound by −3.4 eV. Therefore, we assign the peak at 1.2 eV to the 1S electron, an assignment that is further substantiated by the long lifetime (>100 ps) of this peak.[21] The notable absence of a distinct peak from the 1P electron state is likely due to the fact that most of the QDs are instead excited to exciton states that involve a 1S electron and a corresponding deeper hole in the valence band.[17,32,48,52] In order to significantly populate the 1P electron state, the pump frequency must be resonant with the $1P(e)-1P_{3/2}(h)$ transition.[17,48] Since our pump frequency is fixed at 3.1 eV, it is likely that our pump wavelength is not resonant with the $1P(e)-1P_{3/2}(h)$ transition for any of the QDs in this study. Indeed, a recent report has shown that the photoelectron signal from the 1P electrons appears as a relatively small shoulder on the main photoelectron peak even under resonant 1P pumping conditions.[32] Thus, it is not surprising that we do not resolve a

dx.doi.org/10.1021/nl401309z | Nano Lett. 2013, 13, 2924–2930

distinct peak resulting from the 1P electrons and instead only observe a subtle indication of hot electrons (Supporting Information, Figure S4).

To understand the difference between single excitons in different diameter QDs, we measured the 2PPE spectra of 2.3, 2.5, and 2.8 nm diameter quantum dots under the same experimental conditions. We then normalized the 2PPE spectra by the number of excitons generated in each sample. To avoid multiple carrier generation from an overly intense pump pulse, we set the pulse intensity such that less than 10% of the dots absorb a photon from the pump pulse. The normalized 2PPE spectra per exciton ($I_{\text{PE per exciton}}$) is then calculated as

$$I_{\text{PE per exciton}} = \frac{I_{\text{PE}}}{(N_{\text{QD}}\sigma P)} \quad (1)$$

where I_{PE} is the experimental 2PPE spectrum, N_{QD} is the number density of the quantum dots in solution (which can be calculated from ultraviolet−visible spectra), P is the pump photon flux, and σ is the absorption cross-section of the quantum dots (see details in Supporting Information Section 3).

As shown in Figure 2b, the intensities of the 2PPE spectra decrease as the diameter of the QDs increases from 2.3 to 2.8 nm. For QDs with diameters larger than 2.8 nm, the signal cannot be resolved from the noise level. The shift of the 1S peak due to the energy shift of the band gap is expected to be between 0.1 to 0.2 eV and cannot be resolved in these spectra because the 1S peak is broadened to ∼1.5 eV. There are several factors that could contribute to the broadening of the photoelectron spectral peak, including the size inhomogeneity of the sample as well as the presence of secondary electrons that arise from inelastic scattering.[36] However, we should not experience broadening from charged quantum dots, as has been observed in thin film samples,[25,32] because each laser shot interacts with a new sample of quantum dots. In the future, the secondary photoelectrons that arise due to electron−electron and electron−phonon scattering could be mitigated by using extreme ultraviolet high harmonics as a higher energy probe.[33]

Discussion: Photoelectron Intensity Difference from Quantum Dots of Different Size. The decreasing photoelectron intensity with increasing size of the QDs (Figure 2) can be explained by the decreasing evanescent electron density. The Bohr radius for the CdSe 1S exciton is around 5.6 nm,[48] so intuitively, the exciton orbital extends farther outside as the size of the QDs decreases (Figure 1b). To gain a more quantitative understanding, we performed effective mass model calculations[9,11,12] for the three sizes of quantum dots in our experiment. From these calculations, we obtained the electron wave functions and electron densities (Figure 3) of the 1S exciton. The electron probability distributions (Figure 3a) show two interesting features. First, the smaller quantum dots exhibit a maximum in the electron probability density that is closer to the surface of the QD. Second, the maximum electron density is larger for smaller dots, because the electron wave function has less room to spread inside of the smaller QDs. As a result of both of these factors, the electron density of the larger QDs is relatively low at the surface of the QD.[10−12]

If we consider only the portion of the exciton electronic wave function that extends outside the QD (Figure 3c), we see that the electron density decays to ∼10% of the interface density at distances of 0.1 nm. Much like quantum tunneling through a potential barrier, we see that the chance of finding the electron

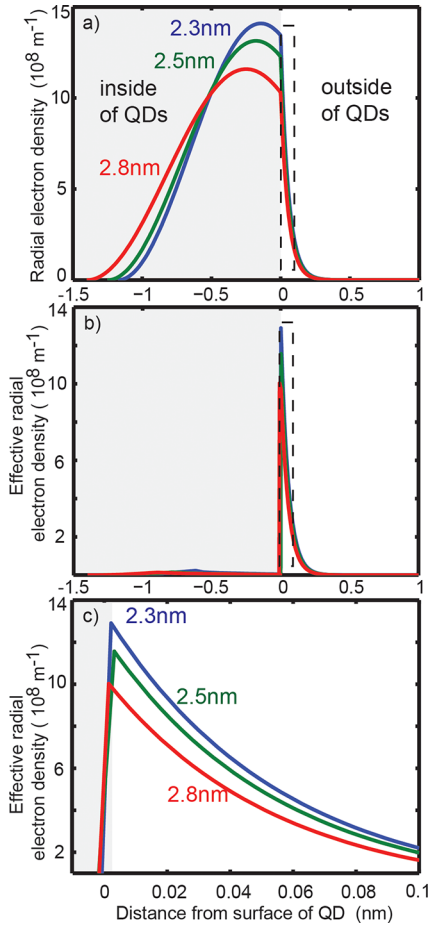

Figure 3. Radial electron probability densities for QDs with various diameters. On the *x*-axis, zero is the surface of the QD. (a) Radial electron probability density in both the interior and exterior of QDs. (b) The effective radial electron density available for photoemission shows that the portion of the electron wave function that extends outside of the QD dominates the photoelectron yield. (c) A magnified view of the effective radial electron probability density outside of the QDs. The difference in the electron density outside of the QD explains the experimentally observed difference in the photoelectron yields.

outside the QD is directly related to the electron probability density at the interface. The probabilities of finding the electron outside the quantum dots are 7.4, 6.7, and 5.6% for the 2.3, 2.5, and 2.8 nm QDs, respectively.

Since the surface of a QD is coated with a layer of ligands, we also need to consider the effect that these ligands will have on a photoelectron emitted from the QD. We consider three ways that the ligands might affect photoemission. (1) The photoelectron could be scattered by the ligands, which can block its path to the vacuum. Surface photoemission of CdSe QDs using soft X-ray radiation from a synchrotron has shown that the photoelectrons originating from the core can effectively penetrate through the ligand layer.[54] Since photoelectrons emitted by soft X-ray photons have even shorter mean free paths than the lower kinetic energy photoelectrons studied here,[27] this suggests that photoelectrons are not blocked by the ligands by scattering. (2) The ligands could affect the excitation of electrons that reside in the portion of the wave function that extends outside of the QD and into the ligand layer. Because the mass of a free electron moving through the ligand layer is very nearly the mass of an electron in vacuum (e.g.,

dx.doi.org/10.1021/nl401309z | Nano Lett. 2013, 13, 2924−2930

octadecylamine ligands do not form bands to which the effective mass approximation can be applied), we can therefore use continuum plane wave functions instead of Bloch wave functions to model the final states in the photoionization process. This increases the likelihood that the electrons outside of the QD will be ionized, as shown in the next paragraph. (3) It is possible that the ligand layer could act as a tunneling barrier for the excited electrons.[55,56] However, since the kinetic energy of the photoelectron is much higher than the height of the barrier, the tunneling barrier should not significantly affect the photoemission process. In short, it is unlikely that the ligands will substantially alter the ionization process of the QD and we therefore neglect the effect the ligand layer in the following analysis.

Conceptually, the photoemission process can be divided into two parts: electrons liberated from the interior of the QDs and electrons liberated from the exterior of the QDs. Following the three-step model of surface photoemission,[26,27] the interior electron is first excited into a Bloch state in the material (Step 1), then experiences electron−electron and electron−phonon scattering while traveling to the surface (Step 2), before finally passing through the interface between material and vacuum (Step 3). Within the three-step model, the probability of photoemission from the interior is limited for the following two reasons. First, in Step 1 the transition from the initial exciton state to the final Bloch state of the material depends on the density of states of the final state.[36] Since hot exciton states are bulklike,[18] we can estimate the density of states based on the bulk, that is, the density of states is proportional to $m_e^{1.5}$, where m_e is the effective mass.[57] The electron effective mass in CdSe is only 13% of the rest electron mass. Therefore, the density of states in CdSe is only 5% of the density of states of the same final states in vacuum (Supporting Information Figure S5). Second, in Step 3 the electrons refract when exiting the QD, and the acceptance cone for low kinetic energy electrons is small. The transmission factor decreases as the initial position of the electron moves closer to the interface and on average is below 0.3 (Supporting Information Section 5). The net result of these two effects is that the probability of photoemission from the interior of the material is significantly reduced, as shown in Figure 3b, which plots the effective electron density available for photoemission after the surface refraction and density of states are taken into account.

In contrast to the interior electrons, the evanescent electrons are intrinsically easier to liberate because they are located on the outside of the QDs and can be ejected into the vacuum directly. Therefore, the photoelectron yield from the evanescent electron should follow Fermi's golden rule, which can be simplified to the integral $\langle \phi_{initial} | r | \phi_{final} \rangle$. Since the final states are free electron wave functions for all three samples, the amount of evanescent electron density in the initial state determines the intensity of the photoelectron yield. Therefore, the increasing evanescent electron densities with smaller QD size (Figure 3) can qualitatively explain the trend of different photoelectron yields (Figure 2). More advanced theoretical calculations will likely be required to achieve precise quantitative agreement with the experimentally observed photoelectron yield.

Our observed connection between the evanescent electron densities and the photoelectron yield agrees well with previous surface photoemission studies using CdSe/ZnS core−shell quantum dots passivated with thiol ligands.[31] In their study, Naaman and co-workers found that smaller QD cores have better coupling to the surface trap states through the shells, and explained this effect as a result of greater extension of the electron densities. In our study, we directly measure the extension of the exciton electronic wave function outside of the QD, and find that the wave function extends farther outside of the QDs in the case of smaller diameter QDs, in agreement with the results of the surface photoemission study[31] discussed above and previous transient absorption studies.[10,11,15,16] Our approach also provides a straightforward and general way to measure the evanescent electron density in the QDs and other nanoparticles.

Interestingly, our finding that the photoelectron yield is inversely proportional to the QD size is a striking demonstration of how photoemission from nanoparticles can be dramatically different from bulk materials. At the surface of bulk materials, the photoemission process must preserve momentum, and as a result, states far outside of the material (such as image potential states) do not have large transition probabilities.[58] However, our results show that the evanescent electron wave function outside of the QDs contributes significantly to the photoelectron signal. This phenomenon can be explained by the following two reasons. First, because the electron wave function is confined by the physical size of the quantum dots, which is around 2.5 nm, the uncertainty in the momentum is 0.2 nm^{-1}, based on the Heisenberg uncertainty principle. The lattice constants of CdSe are a = 0.5 nm and c = 0.7 nm, and the corresponding unit vectors in momentum space are 2 and 1.4 nm^{-1} respectively. Therefore, the momentum uncertainty from the quantum confinement is 10% of the unit vector. This uncertainty in momentum mitigates the conservation of momentum constraints that are normally present in bulk photoemission from surfaces. In addition, the evanescent electron wave function is only 1 Å away from the interface due to quantum confinement, whereas image potential states are typically tens of angstroms away. Moreover, the evanescent electrons are part of the total electron wave function that permeates inside and outside the QD, enabling exchange of momentum with the lattice. Thus, photoemission from small quantum dots resembles that from molecular systems rather than from bulk materials.

Conclusions. By combining a nanoparticle aerosol source with a velocity map imaging spectrometer, we studied two-photon photoelectron spectroscopy from quantum dots with a range of sizes. We found that the photoelectron yield per exciton decreases as the diameter of the quantum dot increases. Using effective mass modeling, we explained this trend as resulting from the different evanescent electron densities that extend outside the surface of the QDs. Thus, we showed that photoelectron spectroscopy of a nanoparticle aerosol provides a straightforward and robust method to compare exciton delocalization in different quantum confined materials. This technique can also be applied to other nanosystems, such as core−shell QDs; however, depending on the specific electronic structure different phenomena are expected. For example, type I core−shell dots would show a substantially reduced photoelectron yield per exciton, because their shell layers typically act as a tunneling barrier for the excited electron to extend out. On the other hand, for type II core−shell QDs in which the electron localizes in the shell the photoelectron yield should increase. Additionally, in this case the kinetic energy of photoelectrons will shift to a lower energy due to the excited electron transfer to a lower lying band following the initial excitation. Overall, by better understanding the various factors

influencing exciton delocalization and coupling, complex nanostructures can be designed for better efficiency of electron transfer.

In the future, photoelectron spectroscopy can provide additional information about the electronic structure of nanomaterials by incorporating electrospray aerosol sources that create physically isolated quantum dots and using higher photon-energy extreme-ultraviolet light sources such as high harmonic generation or synchrotron radiation. When combined with angular information obtained from velocity map imaging techniques, exciton orbitals can be imaged to provide direct fundamental insights into the quantum confined dynamics of quantum dots and other nanoscale systems.

■ ASSOCIATED CONTENT

Supporting Information

(1) UV−vis spectra of quantum dot samples, (2) static and time-dependent two photon photoelectron spectra, (3) calculation of the relative number of excitons in the interaction region, (4) effective mass modeling, and (5) comparison to the photoelectron spectroscopy of bulk materials. This material is available free of charge via the Internet at http://pubs.acs.org.

■ AUTHOR INFORMATION

Corresponding Author

*E-mail: Wei.Xiong@jila.colorado.edu. Phone: (303) 402-6667.

Notes

The authors declare no competing financial interest.

■ ACKNOWLEDGMENTS

The authors acknowledge support from the DOE Office of Basic Energy Sciences (AMOS program) and used facilities provided by the NSF Center for EUV Science and Technology. K.J.S. and G.D. acknowledge support from the Air Force Office of Scientific Research under AFOSR award no. FA9550-12-1-0137. B.B.P. and J.L.J. thank DOE DE-SC0006035 for support. The authors appreciate insightful discussions with Professor M. Aeschlimann, Dr. S. Mathias, Dr. D. B. Strafeld, Dr. P. Matyba, A. V. Carr, C. Chen, Professor D. M. Jonas, Dr. W. K. Peters, and Dr. E. Muller. The authors thank T. Fan for assistance with laser alignment. The authors also thank D. Alchenberger for his help with the UV−vis spectroscopy and ellipsometry measurements and Brad Baxley for the illustration of Figure 1 and the TOC graphic.

■ REFERENCES

(1) Talapin, D. V; Lee, J.-S.; Kovalenko, M. V; Shevchenko, E. V *Chem. Rev.* **2010**, *110*, 389−458.
(2) Nozik, A. J.; Beard, M. C.; Luther, J. M.; Law, M.; Ellingson, R. J.; Johnson, J. C. *Chem. Rev.* **2010**, *110*, 6873−6890.
(3) Kamat, P. V; Tvrdy, K.; Baker, D. R.; Radich, J. G. *Chem. Rev.* **2010**, *110*, 6664−6688.
(4) Wilker, M. B.; Schnitzenbaumer, K. J.; Dukovic, G. *Isr. J. Chem.* **2012**, *52*, 1002−1015.
(5) Choi, C. L.; Alivisatos, A. P. *Annu. Rev. Phys. Chem.* **2010**, *61*, 369−89.
(6) Neumann, O.; Urban, A. S.; Day, J.; Lal, S.; Nordlander, P.; Halas, N. J. *ACS Nano* **2013**, *7*, 42−49.
(7) Loss, D.; DiVincenzo, D. P. *Phys. Rev. A* **1998**, *57*, 120−126.
(8) Kirschbaum, J.; Höhberger, E. M.; Blick, R. H.; Wegscheider, W.; Bichler, M. *App. Phys. Lett.* **2002**, *81*, 280−282.
(9) Schooss, D.; Mews, A.; Eychmüller, A.; Weller, H. *Phys. Rev. B* **1994**, *49*, 72−78.
(10) Zhu, H.; Song, N.; Lian, T. *J. Am. Chem. Soc.* **2010**, *132*, 15038−15045.
(11) Kim, S.; Fisher, B.; Eisler, H.-J.; Bawendi, M. *J. Am. Chem. Soc.* **2003**, *125*, 11466−11467.
(12) Dabbousi, B. O.; Mikulec, F. V; Heine, J. R.; Mattoussi, H.; Ober, R.; Jensen, K. F.; Bawendi, M. G. *J. Phys. Chem.* **1997**, *9463*, 9463−9475.
(13) Lei, K. W.; West, T.; Zhu, X.-Y. *J. Phys. Chem. B* **2013**, *117*, 4582−4586.
(14) Frederick, M. T.; Amin, V. A.; Swenson, N. K.; Ho, A. Y.; Weiss, E. A. *Nano Lett.* **2013**, *13*, 287−292.
(15) Jin, S.; Zhang, J.; Schaller, R. D.; Rajh, T.; Wiederrecht, G. P. *J. Phys. Chem. Lett.* **2012**, *3*, 2052−2058.
(16) Chuang, C.-H.; Doane, T. L.; Lo, S. S.; Scholes, G. D.; Burda, C. *ACS Nano* **2011**, *5*, 6016−6024.
(17) Sewall, S.; Cooney, R.; Anderson, K.; Dias, E.; Kambhampati, P. *Phys. Rev. B* **2006**, *74*, 235328.
(18) Cho, B.; Peters, W. K.; Hill, R. J.; Courtney, T. L.; Jonas, D. M. *Nano Lett.* **2010**, *10*, 2498−2505.
(19) Unold, T.; Mueller, K.; Lienau, C.; Elsaesser, T.; Wieck, A. *Phys. Rev. Lett.* **2005**, *94*, 137404.
(20) Schaller, R. D.; Pietryga, J. M.; Goupalov, S. V.; Petruska, M. A.; Ivanov, S. A.; Klimov, V. I. *Phys. Rev. Lett.* **2005**, *95*, 196401.
(21) Klimov, V.; McBranch, D.; Leatherdale, C.; Bawendi, M. *Phys. Rev. B* **1999**, *60*, 13740−13749.
(22) Gesuele, F.; Sfeir, M. Y.; Murray, C. B.; Heinz, T. F.; Wong, C. W. *Nano Lett.* **2012**, *12*, 2658−2664.
(23) Kambhampati, P. *Acc. Chem. Res.* **2011**, *44*, 1−13.
(24) Hendry, E.; Koeberg, M.; Wang, F.; Zhang, H.; De Mello Donegá, C.; Vanmaekelbergh, D.; Bonn, M. *Phys. Rev. Lett.* **2006**, *96*, 057408.
(25) Miaja-Avila, L.; Tritsch, J. R.; Wolcott, A.; Chan, W.-L.; Nelson, C. A.; Zhu, X.-Y. *Nano Lett.* **2012**, *12*, 1588−1591.
(26) Hufner, S. *Photoelectron Spectroscopy: Principles and Applications*, 3rd ed.; Springer: Berlin, Germany, 2003; pp 349−357.
(27) Damascelli, A. *Phys. Scr.* **2004**, *T109*, 61−74.
(28) Harris, C. B.; Ge, N. H.; Lingle, R. L.; McNeill, J. D.; Wong, C. M. *Annu. Rev. Phys. Chem.* **1997**, *48*, 711−744.
(29) Petek, H.; Ogawa, S. *Prog. Surf. Sci.* **1998**, *56*, 239−310.
(30) Haight, R. *Surf. Sci. Rep.* **1995**, *21*, 275−325.
(31) Xie, Z.; Markus, T.; Gotesman, G.; Deutsch, Z.; Oran, D.; Naaman, R. *ACS Nano* **2011**, *5*, 863−869.
(32) Sippel, P.; Albrecht, W.; Mitoraj, D.; Eichberger, R.; Hannappel, T.; Vanmaekelbergh, D. *Nano Lett.* **2013**, *13* (4), 1655−1661.
(33) Hengleln, A. *J. Phys. Chem.* **1982**, 2291−2293.
(34) Spanhel, L.; Haase, M.; Weller, H.; Henglein, A. *J. Am. Chem. Soc.* **1987**, 5649−5655.
(35) Spanhel, L.; Weller, H.; Henglein, A. *J. Am. Chem. Soc.* **1987**, 6632−6635.
(36) Berglund, C. N.; Spicer, W. E. *Phys. Rev.* **1964**, *136*, 1030−1044.
(37) Liu, P.; Ziemann, P. J.; Kittelson, D. B. *Aerosol Sci. Technol.* **1995**, *22*, 314−324.
(38) Canagaratna, M. R.; Jayne, J. T.; Jimenez, J. L.; Allan, J. D.; Alfarra, M. R.; Zhang, Q.; Onasch, T. B.; Drewnick, F.; Coe, H.; Middlebrook, A.; Delia, A.; Williams, L. R.; Trimborn, A. M.; Northway, M. J.; Decarlo, P. F.; Kolb, C. E.; Davidovits, P.; Worsnop, D. R. *Mass Spec. Rev.* **2007**, *26*, 185−222.
(39) Murphy, D. M. *Mass Spec. Rev.* **2007**, *26*, 150−165.
(40) Wilson, K. R.; Zou, S.; Shu, J.; Ru, E.; Leone, S. R.; Schatz, G. C.; Ahmed, M. *Nano Lett.* **2007**, *7*, 2014−2019.
(41) Zherebtsov, S.; Fennel, T.; Plenge, J.; Antonsson, E.; Znakovskaya, I.; Wirth, A.; Herrwerth, O.; Süßmann, F.; Peltz, C.; Ahmad, I.; Trushin, S. a.; Pervak, V.; Karsch, S.; Vrakking, M. J. J.; Langer, B.; Graf, C.; Stockman, M. I.; Krausz, F.; Rühl, E.; Kling, M. F. *Nat. Phys.* **2011**, *7*, 656−662.
(42) Parker, D. H.; Eppink, A. T. J. B. *J. Chem. Phys.* **1997**, *107*, 2357−2362.
(43) Hickstein, D. D.; Ranitovic, P.; Witte, S.; Tong, X.-M.; Huismans, Y.; Arpin, P.; Zhou, X.; Keister, K. E.; Hogle, C. W.; Zhang,

B.; Ding, C.; Johnsson, P.; Toshima, N.; Vrakking, M. J. J.; Murnane, M. M.; Kapteyn, H. C. *Phys. Rev. Lett.* **2012**, *109*, 073004.
(44) Zhang, X.; Smith, K. a.; Worsnop, D. R.; Jimenez, J. L.; Jayne, J. T.; Kolb, C. E.; Morris, J.; Davidovits, P. *Aerosol Sci. Technol.* **2004**, *38*, 619−638.
(45) Yu, W. W.; Qu, L.; Guo, W.; Peng, X. *Chem. Mater.* **2003**, *15*, 2854−2860.
(46) Pelton, M.; Smith, G.; Scherer, N. F.; Marcus, R. A. *Proc. Natl. Acad. Sci. U.S.A.* **2007**, *104*, 14249−14254.
(47) Galland, C.; Ghosh, Y.; Steinbrück, A.; Hollingsworth, J. A.; Htoon, H.; Klimov, V. I. *Nat. Comm.* **2012**, *3*, 908.
(48) Norris, D.; Bawendi, M. *Phys. Rev. B* **1996**, *53*, 16338−16346.
(49) Dribinski, V.; Ossadtchi, A.; Mandelshtam, V. A.; Reisler, H. *Rev. Sci. Instrum.* **2002**, *73*, 2634−2642.
(50) Tseng, H.-W.; Wilker, M. B.; Damrauer, N. H.; Dukovic, G. *J. Am. Chem. Soc.* **2013**, *135*, 3383−3386.
(51) Smeenk, C. T. L.; Arissian, L.; Zhou, B.; Mysyrowicz, A.; Villeneuve, D. M.; Staudte, A.; Corkum, P. B. *Phys. Rev. Lett.* **2011**, *106*, 193002.
(52) Klimov, V. I. *Annu. Rev. Phys. Chem.* **2007**, *58*, 635−73.
(53) Miaja-Avila, L.; Yin, J.; Backus, S.; Saathoff, G.; Aeschlimann, M.; Murnane, M.; Kapteyn, H. *Phys. Rev. A* **2009**, *79*, 030901.
(54) Borchert, H.; Talapin, D. V.; McGinley, C.; Adam, S.; Lobo, A.; De Castro, a. R. B.; Möller, T.; Weller, H. *J. Chem. Phys.* **2003**, *119*, 1800−1807.
(55) Anderson, N. A.; Lian, T. *Annu. Rev. Phys. Chem.* **2005**, *56*, 491−519.
(56) Pernik, D. R.; Tvrdy, K.; Radich, J. G.; Kamat, P. V *J. Phys. Chem. C* **2011**, *115*, 13511−13519.
(57) Lee, S. J.; Chin, N. H.; Ko, J. J.; Park, M. J.; Kumel, R. *Semicond. Sci. Technol.* **1992**, *7*, 1072−1079.
(58) Hofer, U.; Shumay, I. L.; Reub, C.; Thomann, U.; Wallauer, W.; Fauster, T. *Science* **1997**, *277*, 1480−1482.